JOURNAL OF GUIDANCE, CONTROL, AND DYNAMICS
Vol. 16, No. 4, July–August 1993

Control/Structure Interactions of Space Station Solar Dynamic Modules

Roger D. Quinn*
Case Western Reserve University, Cleveland, Ohio 44106
and
Isam S. Yunis†
NASA Lewis Research Center, Cleveland, Ohio 44135

Potential control/structures interaction problems of large flexible multibody structures in the presence of pointing and tracking requirements are addressed. A control approach is introduced for the simultaneous tracking and vibration control of multibody space structures. The application that is discussed is the planned Space Station Freedom configured with solar dynamic modules. The solar dynamic fine-pointing and tracking requirements may necessitate controller frequencies above the structural natural frequencies of space station and the solar dynamic modules themselves. It is well known that this can give rise to control/structure interaction problems if the controller is designed without giving due consideration to the structural dynamics of the system. Possible control/structure interaction problems of Freedom's solar dynamic power systems are investigated. A finite element model of Freedom is used to demonstrate these potential control/structure interaction problems and the proposed tracking and vibration control approach.

Introduction

THE purpose of this paper is to address potential control/structure interaction (CSI) problems of large flexible multibody structures in the presence of pointing and tracking requirements. The application that is discussed is the planned Space Station Freedom (SSF) configured with solar dynamic (SD) modules.

Solar dynamic electrical power generating modules are being developed for SSF. SSF's initial power source is photovoltaic but SD is essential for the growth of SSF because its efficiency is approximately four times that of the photovoltaic (PV) alternative.[1] An SSF configuration with two SD power systems and eight PV modules is illustrated in Fig. 1. Note that SSF has been redesigned since this work was performed, however, the principles presented here remain applicable. The SD power module is shown in Fig. 2. The concentrator collects and focuses the sun's radiated energy through an aperture into the receiver and, thus, provides the heat energy input for a closed Brayton cycle power system. The SD concentrator-receiver system must be pointed at the sun while its radiator is oriented so that its edge is facing the sun. The SD power system is described in detail by Secunde et al.[1]

"Alpha" and "beta" single-axis revolute joints are used to orient the power modules (PV and SD) toward the sun whereas the station inboard of the "alpha" joints is oriented toward the Earth (see Fig. 1). The two alpha joints operate at the orbital period of about 90 min. A single-axis revolute beta joint between each power module and the station truss permits each power module to rotate with respect to the station truss outboard of the alpha joints. The beta joint axis is normal to the truss longitudinal axis. The beta joints operate at the seasonal frequency.

For SD, precision alignment of the system consisting of the sun, concentrator, and receiver aperture is necessary for optimal power generating efficiency and to prevent thermal damage to the receiver. Hence, two-axis fine-pointing (FP) joints are provided to permit the concentrator to rotate relative to the receiver. In addition to control systems for each of the joints, the station attitude control system uses control moment gyros (CMG) to maintain the orientation of SSF.

SSF's structure is very flexible in comparison to Earth structures, having many natural frequencies below one-tenth of a hertz. The SD fine-pointing and sun-tracking requirements may necessitate controller frequencies above the structural natural frequencies of SSF and the SD modules. It is well known that this can give rise to CSI problems if the controller is designed without consideration of the structure's dynamics.

The most commonly used control law is the proportional integral derivative (PID) controller, the output force of which can be expressed as

$$F = -k(x) - c(v) - I\int x\,dt \tag{1}$$

where k, c, and I are the position, velocity, and integral feedback gains, respectively; and x and v are the sensed position and velocity variables, respectively. Note that the locations of the actuator and three sensors can each be unique. If the sensors and actuators are collocated in space (located on the same relatively rigid body in the same orientation), a PD controller acts as an active spring-damper system attached to

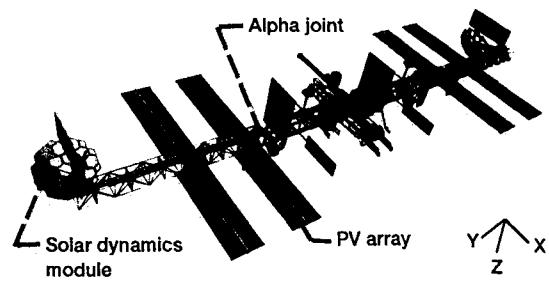

Fig. 1 Space Station Freedom growth configuration.

Presented as Paper 90-3323 at the AIAA Guidance, Navigation, and Control Conference, Portland, OR, Aug. 20–22, 1990; received Feb. 20, 1991; revision received Sept. 20, 1992; accepted for publication Oct. 4, 1992. Copyright © 1990 by the American Institute of Aeronautics and Astronautics, Inc. All rights reserved.

*Associate Professor, Department of Mechanical and Aerospace Engineering. Member AIAA.

†Aerospace Engineer, Structural Systems Dynamics Branch. Member AIAA.

the controlled body. In this case, it is well known that the system is inherently stable given perfect sensors and actuators. Spanos[2] addressed the CSI related effects of sensor dynamics and associated filter dynamics for PD control of flexible spacecraft.

The case of collocation of sensors and actuators also implies that the actuating force and the sensed motion are relative to the same reference frame (body). For example, an actuator can react against (relative to) an attached body; or, on the other hand, an actuator can react (inertially) against expelled fluid or a force field (gravitational or magnetic). In the same way, a sensor can measure relative or inertial motion.

For a linearly flexible structure with control laws of the form of Eq. (1), given relatively stiff actuator and sensor dynamics, instability can be caused by the following[3-5]:

1) In the case of noncollocated sensors, if the controller frequency is in the range of the flexible modes, the controller may excite flexible modes of vibration. The sensed motion may be out of phase with the motion at the actuator so that the actuator excites vibration.

2) In the case of inertial sensing and relative actuation, the actuator can excite its supports or reaction mass. To prevent this, the actuator supports must have relatively high fundamental frequencies compared to the controller bandwidth.

Previous work showed that special attention must be paid to the SD controller design to avoid CSI problems. Previous CSI studies used a NASTRAN model of the SD module mounted on a three bay truss structure which was cantilevered to ground. The FP gimbals were controlled at a rigid-body design frequency of 0.5 Hz and damping ratio of 0.707. The position sensors (sun sensors on the concentrator) were noncollocated with the FP actuators, whereas the rate sensors were collocated. The closed-loop model was found to be unstable. The critical mode was found to have a natural frequency of 2.395 Hz.

One approach to avoid the noted instability is to stiffen the SD structure so that its fundamental component natural frequency is at least twice the FP controller frequency. The radiator is the most flexible component in the SD system. In fact, its fundamental natural frequency of about 0.07 Hz is similar to the fundamental truss-bending frequency of SSF. The drawback with this approach is that the control system design is driving the structural design, perhaps adding unnecessary weight and creating deployment penalties. Also, it was found that increasing the radiator stiffness does not monotonically increase the stability of the system.[5] Changing the control law is a much more practical and reliable alternative. It is possible to design the controller with knowledge of the system's structural dynamics such that it does not cause structural vibrations. In this way, both stability and system performance can be improved with less actuator effort.

In this paper potential CSI problems of the growth configured SSF are demonstrated using a NASTRAN finite element model through closed-loop simulations and eigenanalyses with different sensor and controller configurations. Also, a control approach is introduced for multibody space structures like SSF where both large rigid-body motions and vibratory motions are controlled using the same hardware. This approach is an extension of the approach of Ref. 6 for single flexible bodies. In this way, modules can be targeted and finepointed whereas, simultaneously, disturbance vibrations are damped. The control system is configured to preclude control/structure interactions that might lead to an instability.

Dynamic Modeling of Space Station Freedom

Maneuvers can affect the mode shapes, natural frequencies, and apparent damping characteristics of the structure as well as apply disturbance forces and torques. However, if the rotational maneuver rate is at least an order of magnitude less than the lowest structural natural frequency, then the structural effects are negligible.[7]

For SSF, the maneuvers consist of 1) reboost, translation of the entire structure; and 2) rotation of the main structure to maintain its attitude relative to the Earth on the order of 0.0002 Hz (alpha rotation rate). Note that the power modules orientations are essentially inertially fixed.

The maximum rates of these rotational maneuvers are relatively small, so that we can neglect their structural effects in the eigenanalysis and stability analysis (left side of the equations of motion). Hence, linear finite element modeling at particular joint configurations is sufficient in this case. However, the disturbances to the structure due to the inertial forces during these maneuvers could be of the order of magnitude of the other disturbances and, therefore, should not be neglected in the performance analysis (right side of the equations of motion).

The NASTRAN model of the SSF configuration shown in Fig. 1 that was used in this study was developed by NASA and contained hundreds of modes with natural frequencies below 5 Hz. These hundreds of modes were reduced through modal selection to 149 modes that were found to have the most pronounced effects on the SD modules. Blelloch et al.[8] recently discussed this type of modal representation for control/structure interaction studies. The 149 mode model includes 22 rigid-body modes: six degrees of freedom for the main modules and truss; two degrees of freedom provided by the alpha joints; ten degrees of freedom provided by the PV and SD beta joints; and four degrees of freedom provided by the SD FP joints.

The balance is a set of 127 flexible system modes. Table 1a contains the first 85 natural frequencies in ascending order expressed in hertz. Note the groups of eight repeated frequencies that are associated with the eight PV arrays such as modes 40–47, 52–59, and 70–77. Plots of the mode shapes enabled the categorization of the other modes of interest.

Modeling and Control Theory

A finite element model of the distributed parameter space station can be expressed by the following discrete equations of motion in matrix form:

$$M\ddot{x} + C\dot{x} + Kx = F \tag{2}$$

where M, C, and K are the $N \times N$ mass, damping, and stiffness matrices, respectively; and F and x are the force and displacement vectors, respectively. Actually, C is assumed to be proportional to the K matrix, so that the damped and undamped eigenvectors are identical and only the undamped eigenvalue problem must be solved.

Modal selection permits the reduction of the system order from N to $n \ll N$. Let ω_i^2 and X_i denote the ith eigenvalue and eigenvector pair. A subset X ($N \times n$) of the modal matrix may be selected which includes only those eigenvectors that display relatively greater contributions to the motion of the SD modules. The physical motions of the finite element nodes can be approximately expressed in terms of a subset of modal or natural coordinates by means of the expansion theorem or

$$x \cong Xq \tag{3}$$

The eigenvectors are normalized such that

$$X^T M X = I \tag{4}$$

where I is an $n \times n$ identity matrix. A consequence of this is that

$$X^T K X = \Omega \tag{5a}$$

and

$$X^T C X = Z \tag{5b}$$

where Ω and Z are $n \times n$ diagonal matrices. The elements of Ω are the squares of the natural frequencies ω_i^2 and the elements

Table 1 First 85 open- and closed-loop natural frequencies and damping ratios; in each case, the first three modes are rigid-body translational modes

a) Open loop		b) Closed-loop		
Mode	Nat. Freq., Hz	Mode	Nat. Freq., Hz	Damping Ratio
4	0	4	0.01010342	0.68854
5	0	5	0.01032644	0.69335
6	0	6	0.01037411	0.70621
7	0	7-14	0.03974	0.6314
8	0	15	0.04310934	0.67766
9-16	0	16	0.04500294	0.66892
17	0	17	0.05033278	0.75484
18	0	18	0.05036071	0.75668
19	0	19	0.06294467	0.13902
20	0	20	0.06362111	0.14220
21	0	21	0.07358124	0.00095
22	0	22	0.07611361	0.05184
23	0.07350245	23	0.07642071	0.08169
24	0.07424994	24	0.08817219	0.00511
25	0.07574014	25	0.09409242	0.00591
26	0.07651404	26	0.1010969	0.02747
27	0.07806754	27	0.1031793	0.02856
28	0.08882223	28	0.1206393	0.03835
29	0.09397283	29	0.1308942	0.05488
30	0.1009129	30	0.1330511	0.00303
31	0.1027209	31	0.1479734	0.06401
32	0.1214049	32	0.1587980	0.01176
33	0.1299069	33	0.1589121	0.02463
34	0.1330869	34	0.1641435	0.01711
35	0.1454049	35	0.1641517	0.01733
36	0.1580439	36-43	0.17047	0.2498
37	0.1605129	44	0.1823774	0.00989
38	0.1682609	45	0.2354173	0.03425
39	0.1682809	46	0.2442367	0.06812
40-47	0.1702689	47	0.2528758	1.00000
48	0.1846808	48	0.2967362	0.28062
49	0.2334408	49	0.3048874	0.01084
50	0.2490278	50	0.3110307	0.22195
51	0.2966708	51-58	0.31294	0.0552
52-59	0.3175788	59	0.3162505	0.01732
60	0.3181077	60	0.3169998	0.04938
61	0.3219167	61	0.3213624	1.00000
62	0.3622357	62	0.3661365	0.00490
63	0.3749907	63	0.3986437	0.07544
64	0.3903067	64	0.3991456	0.02850
65	0.4196957	65	0.4012355	0.06181
66	0.4215126	66	0.4176685	0.04391
67	0.4320067	67-74	0.46556	0.06756
68	0.4561986	75	0.4835596	0.01172
69	0.4779116	76	0.4888282	0.02814
70-77	0.4780556	77	0.5342067	0.15841
78	0.5169356	78	0.5549151	0.00115
79	0.5498865	79	0.5907501	0.00207
80	0.5570155	80	0.5941301	0.00295
81	0.5913075	81	0.5966291	0.07287
82	0.5934995	82	0.5980402	0.00985
83	0.6117465	83	0.6827942	0.02978
84	0.6385115	84	0.6846537	0.83247
85	0.6593305	85	0.7127077	0.82926

of Z are $2\zeta_i\omega_i$ where ζ_i is the damping ratio of the ith mode. Inserting Eq. (3) into Eq. (2) and premultiplying by X^T, the reduced order model in natural coordinates can be expressed in matrix form as

$$\ddot{q} + Z\dot{q} + \Omega q = f \tag{6a}$$

$$f = X^T F \tag{6b}$$

or in scalar form

$$\ddot{q}_i + 2\zeta_i\omega_i\dot{q}_i + \omega_i^2 q_i = f_i \qquad i = 1, 2, \ldots, n \tag{7}$$

The modal and physical forces can be partitioned into two parts: control forces and disturbance forces, or $f = f_c + f_d$ and $F = F_c + F_d$. Each actuator is capable of applying a force or torque at certain locations on the structure. The actuator forces are transformed into modal forces through Eq. (6b). Let the truncated modal matrix that only includes the actuated nodes be defined as X_c. Hence, the modal control forces and torques can be expressed as

$$f_c = X_c^T F_c \tag{8}$$

A PID output feedback control law can be expressed as

$$F_c = -\left[G_1 x_m + G_2 \dot{x}_m + G_0 \int x_m \, dt \right] \tag{9}$$

where G_1, G_2, and G_0 are gain matrices and x_m and $\dot{x}_m$ are sensed measurement vectors of displacements and velocities. The gain matrices can cause controller coupling (centralized control) so that each actuator force depends on any or all sensor outputs. The controller is decentralized if each actuating force depends on measurements from only one position sensor, one velocity sensor, and one integrated position sensor. The three sensed measurements could be taken from a single location or from different locations.

Introducing Eq. (9) into Eq. (8), the modal control force can be expressed as

$$f_c = -X_c^T\left[G_1 x_m + G_2 \dot{x}_m + G_0 \int x_m \, dt \right] \tag{10}$$

Letting X_m be defined as that portion of the modal matrix X that corresponds to the measurement locations and introducing Eq. (3) into Eq. (10) the modal control force becomes

$$f_c = -X_c^T G_1 X_m q - X_c^T G_2 X_m \dot{q} - X_c^T G_0 X_m \int q \, dt \tag{11}$$

Introducing Eq. (11) into Eq. (6a), the closed-loop modal equation of motion can be expressed as

$$\ddot{q} + \left[Z + X_c^T G_2 X_m \right]\dot{q} + \left[\Omega + X_c^T G_1 X_m \right] q + X_c^T G_0 X_m \int q \, dt = f_d \tag{12}$$

In general, the natural modes are coupled by the control law so that the closed-loop and open-loop mode shapes are different.[9]

The space station is a collection of flexible bodies connected by joints with actuators at the joints. The actuators couple the various modules of SSF through the joints because in order to apply a force on one body the actuator must react with equal and opposite force against an adjacent body at the joint. Hence, the controllers at the joints reduce the number of rigid-body (zero frequency) modes from 22 to 6. (The attitude controllers further reduce the rigid-body modes of the closed-loop system to three translational modes.) As a consequence, the flexible modes are also coupled so that all of the closed-loop mode shapes may be altered substantially from their open-loop form.

Proportional Integral Derivative Control Gain Design

Control gains can be chosen based on the desired rigid-body performance, that is, pole placement of the rigid-body modes. Let the jth modal gains be defined as g_{1j}, g_{2j}, and g_{0j} for modal position, velocity, and the integral of position. Neglecting structural damping, the closed-loop jth modal equation of motion from Eq. (12) may be expressed as

$$\ddot{q}_j + g_{2j}\dot{q}_j + (g_{1j} + \omega_j^2) q_j + g_{0j} \int q_j \, dt = f_{dj} \tag{13}$$

The characteristic equation for mode j is

$$s^3 + g_{2j}s^2 + (\omega_j^2 + g_{1j})s + g_{0j} = 0 \tag{14}$$

Let the closed-loop eigenvalues be expressed as

$$s_{1,2} = \alpha_j \pm i\beta_j \tag{15a}$$

$$s_3 = \gamma_j \tag{15b}$$

where α_j is the decay rate and β_j the damped natural frequency. The closed-loop characteristic equation can be expressed in the form

$$(s^2 + 2\zeta_{cj}\omega_{cj}s + \omega_{cj}^2)(s - \gamma_j) = 0 \tag{16}$$

where ζ_{cj} and ω_{cj} are the closed-loop damping ratio and natural frequency of mode j. Hence, the closed-loop characteristic values are related according to

$$\alpha_j = -\zeta_{cj}\omega_{cj} \tag{17a}$$

$$\beta_j = \omega_{cj}(1 - \zeta_{cj}^2)^{1/2} \tag{17b}$$

The control gains for mode j required to achieve these eigenvalues are

$$g_{0j} = \gamma_j(\alpha_j^2 + \beta_j^2) \tag{18a}$$

$$g_{1j} = 2\alpha_j\gamma_j + \alpha_j^2 + \beta_j^2 - \omega_j^2 \tag{18b}$$

$$g_{2j} = -(2\alpha_j + \gamma_j) \tag{18c}$$

Equations (18) can be used to determine the modal gains for desired rigid-body pole placement. The feedback gain matrices of Eq. (9) can then be formed based on the modal gains and Eq. (10). This PID control gain design was also developed concurrently by Silverberg and Norris.[10]

The form of the gain matrices, that is, the type of rigid-body modal coupling, depends on the type of feedback: relative or inertial. For example, consider two-single-degree-of-freedom discrete masses which are to be coupled with a position controller. The modal matrix for inertial displacements X_c is a 2×2 identity matrix. If the difference between the two positions is to be fed back to the controller, the gain matrix takes the form

$$G = \begin{bmatrix} g & -g \\ -g & g \end{bmatrix} \tag{19}$$

and the controller acts as a spring between the two masses. If the feedback is on the inertial position of the second mass, the gain matrix takes the form

$$G = \begin{bmatrix} 0 & -g \\ 0 & g \end{bmatrix} \tag{20}$$

The controller acts as a spring to ground for the second mass, but as a disturbance on the first mass, which acts as the reaction mass. The adverse effects of this excitation of parts of a structure that are used as reaction masses are discussed in Ref. 5.

Clearly, in either case, the controller will couple the flexible natural modes. When the sensors are collocated with the actuators and PD control laws are used, the actuators act as springs and dampers at the joints. These active dampers can provide considerable vibration damping to the structure.

Tracking and Vibration Control Approach

Once the gains are determined based on desired rigid-body performance, the vibrations of the resulting closed-loop system will also be controlled with the same actuators. Because of modal coupling as illustrated by Eq. (12), the control gains may need to be adjusted to achieve desired pole placement. This adjustment should be based on the closed-loop system using structural vibration control theory to further enhance overall performance. One candidate vibration control theory is uniform damping control which is straightforward to apply given the discussion of it in the preceding section.[11] This control gain adjustment can increase system performance and reduce required actuator effort. The system controller may be designed in two steps: rigid-body control and vibration control.

Tracking (e.g., the SD module tracking the sun whereas the main modules remain Earth-oriented) requires relative rigid-body motions and can be achieved using inertial navigation sensors such as sun sensors. The inertial information can be fed back to joint controllers so that the effective null "stretch length" of the "active spring" changes accordingly. With this in mind, the feedback control torque for a joint can be expressed as

$$\tau = -k(\theta - \theta_0) - c(\omega - \omega_0) - I\int(\theta - \theta_0)\,dt \tag{21}$$

where θ and ω are the sensed angular displacement and velocity of a module (or the difference between the two adjacent modules that the joint connects), respectively; and θ_0 and ω_0 are the desired angular displacement and velocity which can be time varying. The control gains, k, c, and I, can remain constant or can be time varying based on rigid-body motions. The tracking (and, hence, time rate of change of θ_0 and ω_0) will be at a relatively slow rate (90-min orbit period) compared to the structural frequencies and vibration controller frequencies. In fact, as discussed in the second section, ω_0 is orders of magnitude slower than the structural frequencies and, hence, can be considered essentially zero for the purposes of vibration analysis. Hence, these control gains may be chosen based on rigid-body performance as in Eqs. (18).

Table 2 Velocity and position gains for rigid-body pole placement

Structure DOF	Velocity, lb*s/in.	Position, lb/in.
SS rotation x	2.20252 E+08	0.98849 E+07
SS rotation y	2.74866 E+07	1.23359 E+06
SS rotation z	0.23570 E+09	1.05970 E+07
Alpha joints	5.55083 E+06	0.99648 E+06
PV beta joints	0.14976 E+05	0.26618 E+04
SD beta joints	4.23093 E+05	7.59535 E+04
FP gimbal inner	3.85542 E+06	8.65155 E+06
FP gimbal outer	3.35542 E+06	7.70155 E+06

Stability Analysis Results

A stability analysis was conducted to demonstrate CSI issues. Note that we have chosen to neglect structural damping for the stability analysis. In this way, any destabilizing or stabilizing effects will be readily apparent and will not be masked by ad hoc structural damping. Structural damping tends to improve system stability, hence, this is a limiting case.

Table 2 contains the velocity and position gains for the 19 PD controllers. These gains were chosen based on collocated PD control laws and pole placement of the 19 rotational rigid-body modes such that the system displayed the closed-loop rigid-body eigenvalues shown in Table 3. At the time that this research was performed, the baseline-design control bandwidths for the space station were listed as 0.01 Hz for the inertial navigation system, 0.04 Hz for the alpha joints and for the beta joints, and 0.5 Hz for the SD fine-pointing joints. The damping ratios were listed as 0.707 for all controllers. The closed-loop system has three rigid-body (translational) modes. (Subsequent work has shown that SSF control moment gyros may not be capable of attaining the 0.01 Hz bandwidth.[12])

These collocated PD controllers were applied to the flexible SSF model. The resulting closed-loop eigenvalues are shown in Table 1. Comparing Tables 1 and 3, we see that the rigid-body eigenvalues are noticeably altered. This is not surprising because the FP controller bandwidths are well above many of the

Table 3 Rigid-body collocated controller design

Function	Mode	Nat. Freq., Hz	Damping ratio
Station	4	0.01002656	0.69479
rotations	5	0.01016634	0.70528
	6	0.01024282	0.71472
Alpha	7	0.03988495	0.72386
joints	8	0.04045301	0.73716
PV beta	9-16	0.03818168	0.67487
SD beta	17	0.04388041	0.76608
joints	18	0.04393031	0.76793
SD FP	19	0.4985832	0.70649
	20	0.5001788	0.70552
	21	0.5017476	0.70873
	22	0.5049748	0.71391

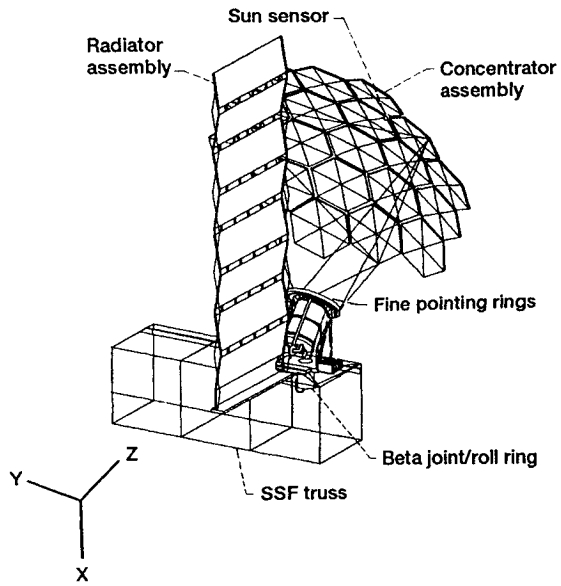

Fig. 2 Solar dynamic power module.

structural frequencies. Some modes are critically damped (or overdamped), for example, modes 47 and 61. Also note that the joint controllers provide considerable damping to the flexible modes. For instance, the PV open-loop mode numbers 40-47, 52-59, and 70-77 correspond to closed-loop numbers 36-43, 51-58, and 67-74, respectively. The frequencies are only slightly changed but the damping provided by the controllers is quite significant at 25, 5.5, and 6.7%, respectively. In fact, the majority of the flexible modes are damped at least a few percent. Hence, we see that the joint controllers act as vibration dampers as well as couple the rigid-body modes. Control spillover into the flexible modes is beneficial.

Although the preceeding analysis is encouraging, collocated control may not be practical for pointing the power modules. The joints controllers provide internal torques but pointing the power modules requires sensing of the sun's position which is inertially fixed. For example, sun sensors on the concentrators can measure x and y rotations of the concentrators relative to the sun where the z axis is normal to the sun. In the joint configuration of this dynamic model, the inner FP ring gimbal axis aligns nominally with the y axis (SSF truss longitudinal axis) and the outer FP ring axis aligns nominally with the line formed by $-0.6x + 0.8z$. A controller similar to the collocated controller already given was formed, except the FP position sensing was taken from the sun sensors: $-x$ to the outer ring and y to the inner ring. The velocity feedback remained collocated at the FP gimbals. This configuration had three unstable modes: 0.1764, 0.1767, and 0.4037 Hz with damping ratios of -0.04, -0.04, and -0.007, respectively.

Clearly in the preceding case, the outer ring position controller is missing the z axis feedback information. To check

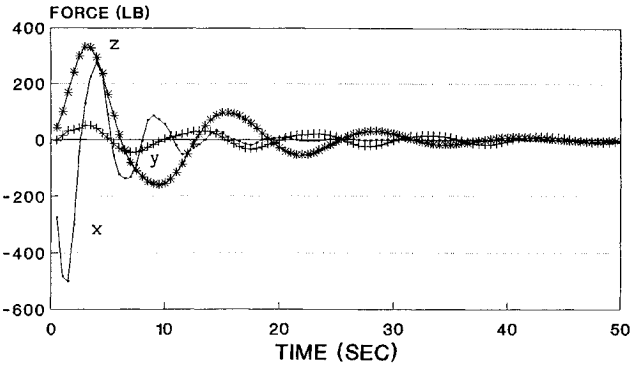

Fig. 3 Docking forces on Space Station.

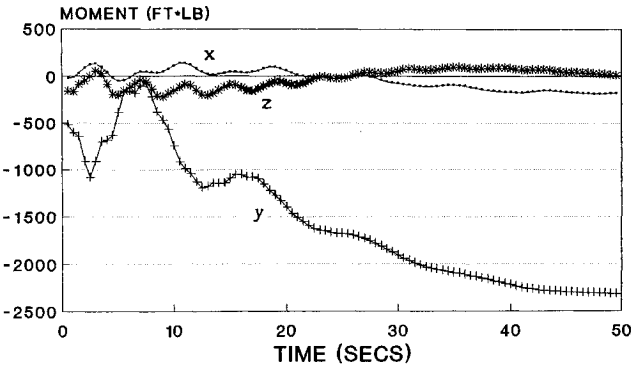

Fig. 4 Docking moments on Space Station.

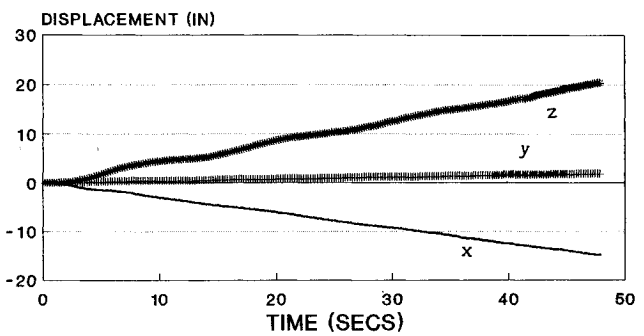

Fig. 5 Translation of the center of mass of Space Station.

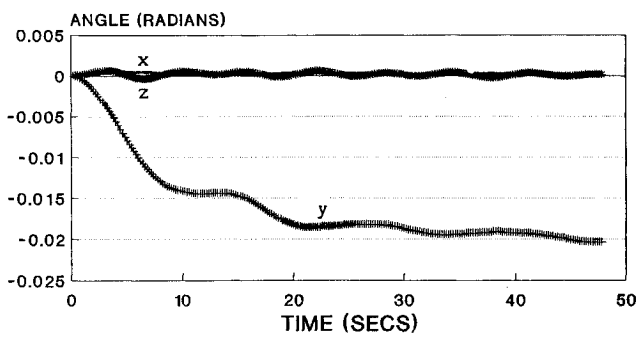

Fig. 6 Rotation of the habitation modules.

this we assumed the existence of z inertial rotational sensors on the port concentrator and formed a controller the same as earlier but with position feedback to the outer ring of $-0.6x + 0.8z$. This closed-loop system was found to be stable. Hence, we see that the already noted instability is a result of improper feedback due to the lack of a sensor to measure the z rotations (an observability problem) and that noncollocation is not a problem.

Finally, a controller was formed such that the feedback to the port FP rings for position and velocity was taken from x, y, and z oriented sun sensors. In this case, the closed-loop system was found to be unstable at 2.2597 Hz with a damping ratio of -0.003. A small amount of structural damping (typically taken to be 0.5%) is enough to stabilize the system. This instability is caused by the noncollocated FP sensor-actuator arrangement. We believe that damping from the alpha and beta joints prevent a greater degree of instability in this case. For brevity we have not included tables of eigenvalues for the last three cases, but a summary of the stability analysis is shown in Table 4. Note that collocated velocity feedback stabilizes the system in which noncollocated position feedback was used.

Simulations of Space Station Freedom

Numerical simulations of SSF were conducted to demonstrate the tracking and vibration control approach using the control gains of Table 2 which are based upon rigid-body pole placement. Motions at various points were plotted vs time during a Shuttle docking at the primary docking location. The input docking forces and moments (Figs. 3 and 4) are worst case docking forcing functions. Note that after docking, the Shuttle is attached to SSF and substantially alters the dynamic model. However, we have neglected this effect in the simulations.

To demonstrate the need for tracking control applied at the joints, collocated vibration control was applied initially at all of the joints without tracking control. Each of these vibration controllers uses relative sensing across the joint and attempts to minimize this relative motion. This is equivalent to applying torsional springs and dampers at each of the joints. In this case, pointing of the power modules can only be accomplished by the space station attitude controllers because it is the only control system which makes use of inertial sensing.

Docking causes SSF's center of gravity (c.g.) to translate and rotate significantly as shown in Figs. 5 and 6, respectively.

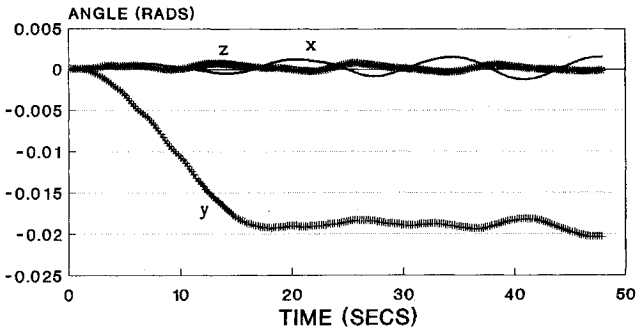

Fig. 7 Port concentrator rotation with collocated control.

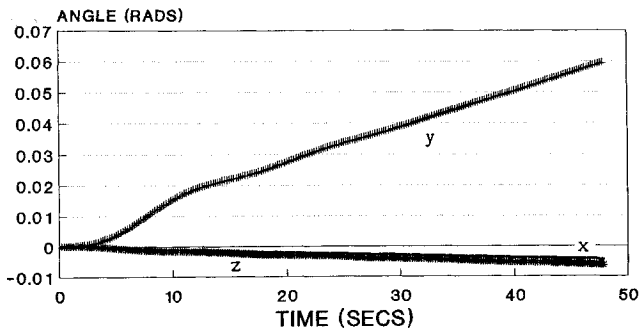

Fig. 8 Port concentrator rotation with no FP control.

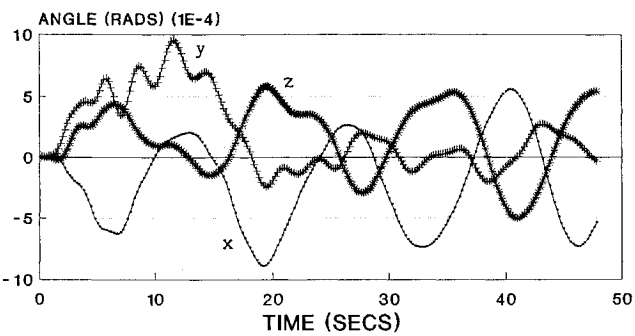

Fig. 9 Port concentrator rotation using inertial sensors at the concentrator as feedback to the FP controllers.

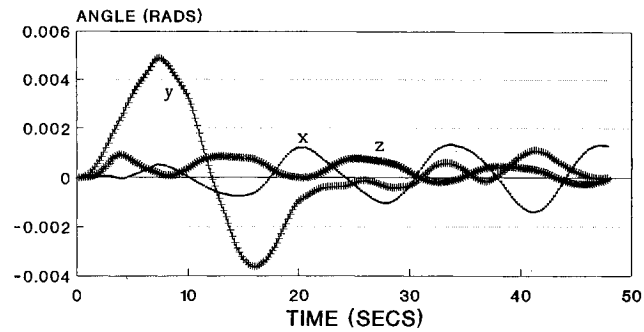

Fig. 10 Port concentrator rotation using station inertial navigation sensor feedback to the FP controllers.

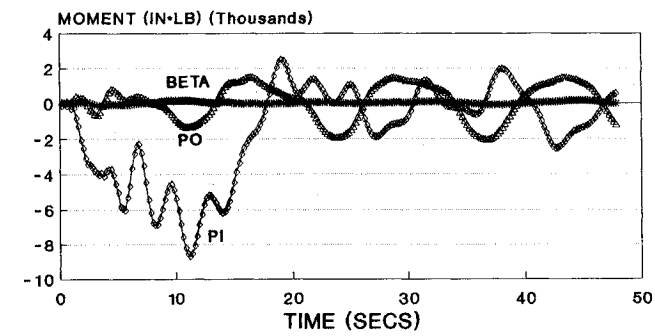

Fig. 11 Port SD control moments for tracking control.

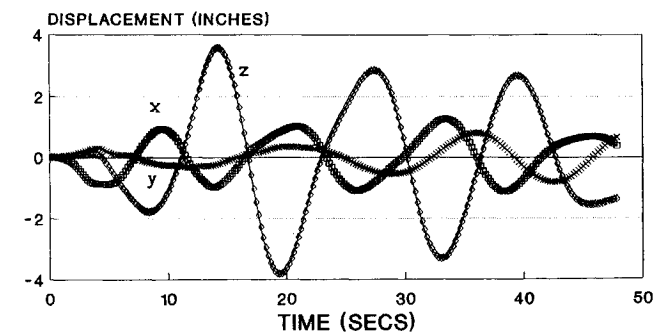

Fig. 12 Radiator tip displacement during tracking control.

Table 4 Stability analysis summary: fine-pointing joints controlled using sensors at different locations and in different controller configurations

Case	Sensor location: Position	Sensor location: Rate	Stability	Critical freq., Hz	Damping ratio
1	Coll.[a]	Coll.	Stable		
2	Conc.[b]	Coll.	Unstable	0.1764	−0.0419
	x, y	Coll.		0.1767	−0.0423
				0.4037	−0.0070
3	Conc. x, y, z	Coll.	Stable		
4	Conc. x, y, z	Conc. x, y, z	Unstable	2.2597	−0.0032

[a]Coll. = collocated. [b]Conc. = inertial sensors on concentrator.

However, for SD we are most interested in the orientation of the concentrator with respect to the sun. Precise pointing specifications were not defined when this research was conducted but a good rule is that the concentrator should be pointed within 0.1 deg at all times for best SD performance. With collocated vibration control and no tracking control, the concentrator rotation very nearly followed the c.g. rotations as expected. The y axis pointing is off by about 1 deg (0.02 rad) for more than 30 s as can be seen in Fig. 7. Tracking control is clearly needed because the station attitude control system cannot respond quickly enough to damp the motions caused by docking.

As an additional check of the simulation and of the need for tracking control, next the FP control was disabled such that the FP gimbals were free to rotate. In this case, the rotation of the receiver and supporting structure caused the concentrator to rotate as shown in Fig. 8. The c.g. of the concentrator remained fixed and its supporting truss acted as a moment arm to rotate it away from its desired orientation.

Based on the preceding, tracking control is clearly needed in order to point the power modules during docking. If we measure the inertial orientation (x, y, z) of the concentrator (preferably near the gimbals), we can feedback this angular position information to the gimbal ring controllers for tracking control as in case 3 of the stability analysis. (Note that collocated velocity feedback is used.) This case is illustrated in Fig. 9; pointing is maintained within 0.06 deg (0.001 rad) during docking.

If we do not have a direct measure of the inertial orientation of the concentrator, we can use SSF's main inertial guidance sensing information as in Eq. (21). In this case, $-\theta_0$ is the station's inertial orientation and θ is the difference between the gimbal ring orientation and its supports. The sum $\theta + \theta_0$ is an approximation of the inertial rotation of the concentrator supports. Note that SSF's motion θ_0 is guaranteed to be relatively slow because of its large inertia. The concentrator orientation error is illustrated in Fig. 10. The maximum off pointing is less than 0.29 deg (0.005 rad). The error is due to the difference in orientation between the main modules and the SD supports caused by the alpha and beta joints and flexible motions. Hence, we conclude that concentrator pointing can be maintained during severe docking maneuvers without additional inertial sensors. The FP control moments required for tracking are illustrated in Fig. 11.

Because we are using a decentralized control strategy, pointing of SD is independent of the station attitude. Hence, substantially reducing the bandwidth of the attitude control system as suggested in Ref. 15 will not significantly affect the pointing performance of SD.

Radiator tip flexible vibration is shown in Fig. 12 for the station tracking case. Note that this 4-in. vibration amplitude (the largest of any point on the radiator) is at the tip of the cantilevered radiator which is over 60 ft long. This vibration should be acceptable. Note that the fundamental frequency of vibration (from Fig. 12) is about 0.07 Hz which corresponds to the fundamental truss and radiator bending frequencies.

Conclusions

The actuators at the joints couple the 16 component rigid-body modes of the space station. As a consequence, the flexible modes are also coupled so that all of the closed-loop modes can be altered substantially from their open-loop form. The closed-loop eigenvalues including and excluding the flexible modes in the model are noticeably different because of the coupled control approach. The structural damping of the flexible modes is augmented considerably by the controllers, which inherently act as vibration dampers. The system controller can be designed in two steps: rigid-body control and vibration control. Collocated decentralized PD controllers with relative sensing and actuating act as "active springs and dampers" and are inherently stabilizing. A noncollocated decentralized controller can be considered "unnatural" since there is no mechanical analog and it is inherently destabilizing. Inertial sensing with relative actuation is inherently destabilizing, because a part of the structure is used as a reaction mass. However, if collocated velocity feedback is used in conjunction with inertial sensing, controller bandwidths that are higher than the natural frequencies of components attached to the reaction mass may be permissible. This is the case for fine-pointing control of the SD concentrator relative to the SD receiver with a very flexible radiator attached to the receiver. Tracking control, using inertial orientation sensors on the concentrator or the station inertial guidance sensors, was found to be stable and effective for pointing the concentrator. The radiator flexible motion was found to be relatively small during the most severe Shuttle docking maneuver.

Acknowledgments

This work was funded by Grant NAG3-1099 from the Solar Dynamic Power Branch, NASA Lewis Research Center. This support was greatly appreciated. The NASTRAN model of Space Station Freedom was supplied by NASA Lewis Engineering Directorate. The shuttle docking loads were supplied by NASA/JSC Loads and Structural Dynamics Branch.

References

[1]Secunde, R., Labus, T. L., and Lovely, R. G., "Solar Dynamic Power Module Design," *Proceedings of the 24th International Energy Conversion Engineering Conference*, Vol. 1, IEEE, Piscataway, NJ, pp. 299-307.

[2]Spanos, J. T., "Control-Structure Interaction in Precision Pointing Servo Loops," *Journal of Guidance, Control, and Dynamics*, Vol. 12, No. 2, 1989, pp. 256-263.

[3]Gevarter, W. B., "Basic Relations for Control of Flexible Vehicles," *AIAA Journal*, Vol. 8, No. 4, 1970, pp. 666-672.

[4]Meirovitch, L., *Dynamics and Control and Structures*, Wiley, New York, 1990.

[5]Quinn, R. D., and Yunis, I. S., "Control/Structure Interactions of Freedom's Solar Dynamic Modules," *Proceedings of the AIAA Guidance, Navigation, and Control Conference* (Portland, OR), AIAA, Washington, DC, Aug. 1990, pp. 79-88.

[6]Quinn, R. D., and Meirovitch, L., "Maneuver and Vibration Control of SCOLE," *Journal of Guidance, Control, and Dynamics*, Vol. 11, No. 6, 1988, pp. 542-553.

[7]Meirovitch, L., and Quinn, R. D., "Equations of Motion of Maneuvering Flexible Spacecraft," *Journal of Guidance, Control, and Dynamics*, Vol. 10, No. 5, 1987, pp. 453-465.

[8]Blelloch, P. A., Young, J. W., and Carney, K. S., "Modal Representations in Control/Structures Interaction," *Proceedings of 1989 American Control Conference* (Pittsburgh, PA), June 21-23, 1989, pp. 2802-2807.

[9]Meirovitch, L., and Silverberg, L. M., "Globally Optimal Control of Self-Adjoint Distributed Systems," *Optimal Control Applications and Methods*, Vol. 4, 1983, pp. 365-386.

[10]Silverberg, L., and Norris, M. A., "Self-Tuning Algorithms for Uniform Damping Control of Spacecraft," *Proceedings of the AIAA/ASME/ASCE/AHS/ASC 31st Structures, Structural Dynamics, and Materials Conference* (Long Beach, CA), AIAA, Washington, DC, April 2-4, 1990, pp. 2427-2436.

[11]Silverberg, L., "Uniform Damping Control of Spacecraft," *Journal of Guidance, Control, and Dynamics*, Vol. 9, No. 2, 1986, pp. 221-227.

[12]Wie, B., et al., "New Approach to Attitude/Momentum Control for the Space Station," *Journal of Guidance, Control, and Dynamics*, Vol. 12, No. 5, 1989, pp. 714-722.